ChemComm

COMMUNICATION

View Article Online
View Journal | View Issue

Cite this: *Chem. Commun.*, 2024, **60**, 6292

Received 24th April 2024,
Accepted 24th May 2024

DOI: 10.1039/d4cc01950d

rsc.li/chemcomm

Photocatalytic CO_2 reduction with iron porphyrin catalysts and anthraquinone dyes†

Huiqing Yuan,*[ab] Yuanhai Yu,[b] Shuang Yang,[b] Qinqin Lei,[b] Zhiwei Yang,[b] Bang Lan*[a] and Zhiji Han *[b]

Herein we studied visible-light-driven CO_2 reduction using a series of tetra-phenylporphyrin iron catalysts and inexpensive anthraquinone dyes. Varying the functional groups on the phenyl moieties of the catalysts significantly enhances the photocatalytic activity, achieving an optimal turnover number (TON) of 10 476 and a selectivity of 100% in the noble-metal-free systems. The highest activity found in a bromo-substituted catalyst is attributed to favorable electron transfer from the photosensitizer to the iron porphyrin.

The development of artificial photosynthetic systems for converting solar energy into renewable chemicals is one of the long-standing goals in chemical society.[1] Photocatalytic reduction of CO_2 into value-added chemicals is a promising avenue for both utilizing sunlight and closing the anthropogenic carbon cycle.[2] Over the past few decades, significant advancements have been made in homogeneous photocatalytic CO_2 reduction. However, the majority of these systems have predominantly employed complexes with precious metals (such as Ru, Ir, and Re) as either photosensitizers or catalysts.[3] The development of photocatalytic systems with high activity and selectivity using abundant elements poses a significant challenge, yet it is crucial for advancing photocatalytic CO_2 reduction technologies.[4]

Recently, a series of non-noble metal complexes have been reported as active catalysts in noble-metal-free systems for photocatalytic CO_2 reduction.[5] For instance, a cobalt quaterpyridine complex was shown to catalyze CO_2 to CO with a high turnover number (TON) of 19 000 using an organic triazatriangulenium salt as the photosensitizer (PS).[5a] Pyridinethiolate Ni(II) complexes have shown high activity in converting CO_2 to HCOOH.[5b] This system achieved a TON_{Ni} of 14 000 in 10 h when using eosin Y as the organic PS. Advancements have also been made with terpyridine-based iron complexes in conjunction with 4CzIPN dyes.[5c] Other molecular catalysts such as Fe,[5d–f] Co,[5g,h] Ni,[5i] or Mn,[5j] have been found to reduce CO_2 to CO when employing copper diimine diphosphine PSs, achieving TONs up to 11 800 under optimal conditions.[5h]

Iron porphyrin complexes were initially studied as one of the most efficient classes of molecular electrocatalysts for CO_2 reduction to CO.[6] Later, Robert and Bonin reported that the iron tetraphenylporphyrin complexes functionalized with trimethylammonio groups and **Fe2** were also active in photocatalytic systems for reducing CO_2 to CO and/or CH_4, with TONs ranging from 79 to 367.[3k] In our laboratory, we found that **Fe2** exhibited exceptional activity in photocatalytic CO_2 reduction, achieving a TON as high as 21 616 when using a copper purpurin complex or aminoanthraquinone dyes as the PSs.[7] A recent study from the Cautsolelos and Charalambidis groups showed that fluorine and trimethylammonium substituted porphyrins are highly active for photocatalytic CO_2 reduction, achieving up to 5500 TONs.[8] In this study, to unravel factors that govern activity for the development of advanced photocatalytic systems, we present a systematic structure–function study using iron porphyrins with different electronic substituents on the meso-phenyl backbone (Fig. 1). Our results show that the porphyrin with more electron-withdrawing groups exhibits higher activity in photocatalytic CO_2 reduction, suggesting that the reduction steps either from Fe(I) to Fe(0) or from Fe(II)–CO_2 to Fe(I)–CO_2 are rate-limiting in catalysis.

The bromo and methyl substituted porphyrins were synthesized *via* condensation of the corresponding benzaldehyde and pyrrole following hydrolysis (ESI†). The methoxy and hydroxy versions of porphyrins were characterized using nuclear magnetic resonance (NMR) spectroscopy (Fig. S1–S4, ESI†) and high-resolution mass spectrometry (HRMS) (Fig. S7 and S8, ESI†). Iron porphyrins **Fe1** and **Fe3** were prepared from the corresponding porphyrins and $FeCl_2{\cdot}4H_2O$ in methanol at 50 °C for 48 hours. The maximum absorption wavelengths for **Fe1**, **Fe2**, and **Fe3** are all located at 416 nm in *N*,*N*-dimethylformamide (DMF), with molar extinction coefficients of 97 550 M^{-1} cm^{-1},

[a] *School of Chemistry and Environment, Jiaying University, Meizhou, Guangdong 514015, China. E-mail: yuanhq3@mail2.sysu.edu.cn, jyulb6@163.com*
[b] *MOE Key Laboratory of Bioinorganic and Synthetic Chemistry, School of Chemistry, Sun Yat-sen University, Guangzhou 510275, China. E-mail: hanzhiji@mail.sysu.edu.cn*

† Electronic supplementary information (ESI) available. See DOI: https://doi.org/10.1039/d4cc01950d

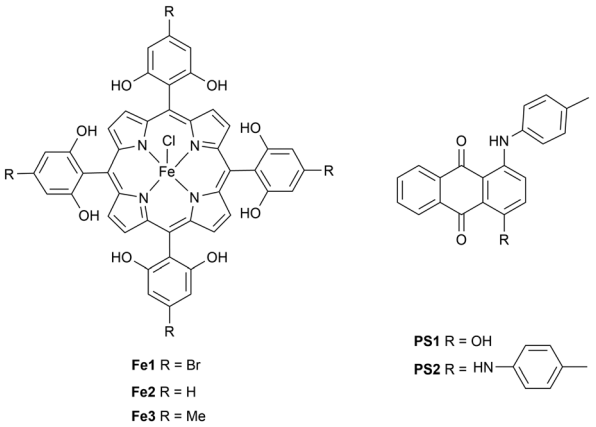

Fig. 1 Structures of PSs and catalysts in the study.

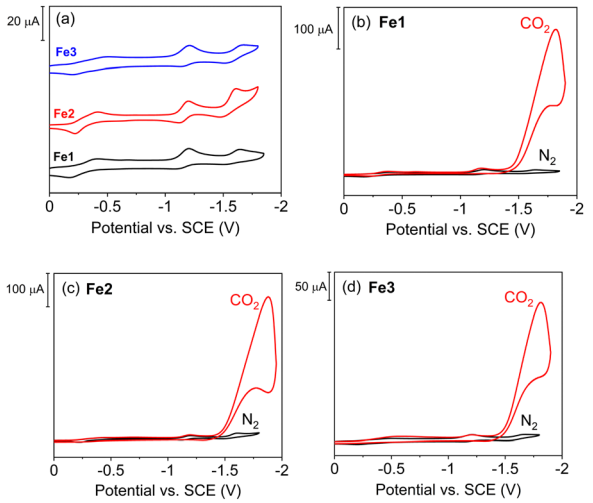

Fig. 2 (a) Cyclic voltammograms of 1.0 mM **Fe1** (black), **Fe2** (red) and **Fe3** (blue) in 5 mL DMF containing 0.1 M $TBAPF_6$ under N_2; (b), (c), and (d) 1 mM catalyst under N_2 (black) and CO_2 (red).

87 370 M^{-1} cm^{-1}, and 64 210 M^{-1} cm^{-1}, respectively (Table 1 and Fig. S9–S11, ESI†).

Cyclic voltammograms (CVs) recorded in DMF under N_2 (Fig. 2a and Table S1, ESI†) showed that the reduction potentials of the $Fe^{III/II}$ couples exhibited cathodic shifts in the order of **Fe1**, **Fe2**, and **Fe3**, which is consistent with increasing electron-donating properties of the porphyrin ligands. However, their $Fe^{II/I}$ and $Fe^{I/0}$ redox couples are both at similar potentials (Fig. 2a). To investigate these complexes for CO_2 reduction, CVs were performed in CO_2-saturated DMF (Fig. 2b–d). Consistent with the results reported for **Fe2**,[6b] both **Fe1** and **Fe3** displayed significant increase in currents in the presence of CO_2 at potentials corresponding to the $Fe^{I/0}$ couples, suggesting that all three iron porphyrins are active catalysts for CO_2 reduction. Compared with **Fe2**, the onset catalytic potential slightly shifts from −1.44 V to −1.42 V for **Fe1** and to −1.46 V for **Fe3** (Table 1 and Fig. S12, ESI†).

To study the activity of iron catalysts in noble-metal-free photocatalytic systems, we selected two inexpensive anthraquinone dyes 1-hydroxy-4-[(4-methylphenyl)amino]-9,10-anthraquinone (**PS1**) and 1,4-bis[(4-methylphenyl)amino]-9,10-anthraquinone (**PS2**) as the PSs (Fig. 1). UV-vis spectroscopy showed that these two anthraquinones displayed high molar extinction coefficients (11 230 M^{-1} cm^{-1} for **PS1** and 16 550 M^{-1} cm^{-1} for **PS2**) at the visible region (Fig. S13 and S14, ESI†). In addition, CVs of **PS1** and **PS2** both exhibited reversible reduction waves at −0.733 V and −0.885 V, respectively (Fig. S19, ESI†). Although 1-amino-2-bromo-4-hydroxy-9,10-anthraquinone has been reported by our laboratory as one of the most active organic dyes for CO_2 reduction, it is over 3900 times more expensive (based on Sigma Aldrich prices in 2024) compared with **PS1** and **PS2**.

Photocatalytic CO_2 reduction was conducted in CO_2-saturated DMF (5 mL) containing the anthraquinone PS, iron porphyrin catalyst, and 1,3-dimethyl-2-phenyl benzimidazoline (BIH) as the sacrificial reductant, under irradiation by a blue light-emitting diode (LED). The use of blue LEDs in our study was based on the absorption spectra of the reduced anthraquinones observed in our previous study.[7b] Gas chromatography was used to monitor the gaseous products generated from the systems. In our experiments, no H_2 was observed throughout the catalytic process and the selectivity for the reduction of CO_2 to CO reached 100%.

Optimization of the photocatalytic system was achieved by varying the concentration of each component. With fixed concentrations of BIH (30 mM) and **Fe1** (1 μM), increasing the concentration of **PS1** led to a higher overall yield of CO (Fig. S20, ESI†). However, no further increase in activity was observed when the [**PS1**] exceeded 0.2 mM. When the [**PS1**] and [**Fe1**] were fixed at 0.2 mM and 1.0 μM, respectively, altering the [BIH] showed increase in activity up to 30 mM (Fig. S21, ESI†).

Under the optimal conditions (0.2 mM **PS1**, 1 μM **Fe**, and 30 mM BIH), the system's activity followed an order of **Fe1** > **Fe2** > **Fe3** (Fig. 3a and Table 1). When using **PS1**, the amounts of CO produced after 10 hours of illumination were 50.3 μmol (for **Fe1**), 25.6 μmol (for **Fe2**), and 21.5 μmol (for **Fe3**), corresponding to TONs (*vs.* Fe) of 10 052, 5115, and 4305, respectively. When employing **Fe1** as a catalyst, **PS1** exhibited higher activity for the photocatalytic reduction of CO_2 to CO compared with

Table 1 Photophysical, electrochemical, and photocatalytic CO_2 reduction of catalyst

Cat	λ_{max} abs/nm (ε M^{-1} cm^{-1})	Onset catalytic potential (V *vs.* SCE)[a]	CO[b] (μmol)$_1$	CO[c] (μmol)$_2$	TON$_1$[b]	TON$_2$[c]	Φ[d]
Fe1	97 550	−1.42	50.3	25.6	10 052	5112	0.95%
Fe2	87 370	−1.44	25.6	17.6	5115	3519	0.63%
Fe3	64 210	−1.46	21.5	16.6	4305	3330	0.43%

[a] Under CO_2 atmosphere. [b] 1 μM catalyst, 0.2 mM **PS1** and 30 mM BIH. [c] 1 μM catalyst, 0.2 mM **PS2** and 30 mM BIH. TON = n(CO)/n(catalyst). [d] 5 μM catalyst, 0.2 mM **PS1** and 30 mM BIH, λ = 450 nm, Φ calculated in 2 h.

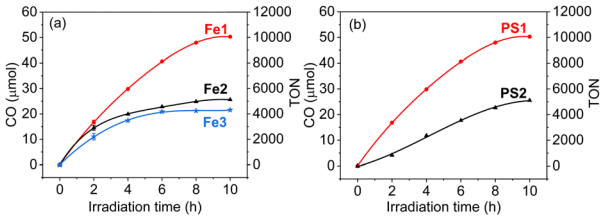

Fig. 3 CO generation in CO_2-saturated DMF solutions containing (a) 30 mM BIH, 1.0 μM catalyst, 0.2 mM **PS1**; (b) 30 mM BIH, 1.0 μM **Fe1**, 0.2 mM **PS1** and **PS2** under blue LED.

PS2 (Fig. 3b). Analysis of the electrochemical data for **PS1** and **PS2** (Table S2 and Fig. S19, ESI†) shows that the –PhMe group acts as an electron-donating group while the –OH group is electron-withdrawing on AQ. These distinct electronic groups may create an internal donor–acceptor property by desymmetrizing the organic molecule, which facilitates electron-transfer of the dye.[7b] Employing **Fe1** as the catalyst, CO quantum yields of 0.95% with **PS1** and 0.72% with **PS2** were obtained at a wavelength of 450 nm.

A series of control experiments was conducted to investigate the nature of the system. The absence of the catalyst, PS, BIH, or light resulted in no generation of CO (Table S3, ESI†). To study the source of CO, photolysis experiments performed in an atmosphere of $^{13}CO_2$ produced exclusively ^{13}CO as determined by GC-MS analysis (Fig. S24, ESI†). Moreover, no CO was observed from experiments performed under a nitrogen atmosphere (Table S3, entry 8, ESI†). These results thus suggested that CO originated from the reduction of CO_2.

In addition, dynamic light scattering (DLS) and mercury poisoning experiments were employed to evaluate the system's homogeneity. DLS results revealed the absence of nanoparticles in both the pre-catalytic and post-catalytic systems (Fig. S25, ESI†). The introduction of excess of Hg^0 to the system showed identical photocatalytic activity (Fig. S26, ESI†), which ruled out contaminants from amalgam-forming metals. These findings suggest that the photocatalytic system in our study is homogeneous.

To investigate the photochemical mechanism, UV-vis spectroscopy was utilized. The UV-vis results (Fig. S27 and S28, ESI†) revealed no spectral change in the photosensitizer by adding BIH and **Fe1**, which rules out a static quenching mechanism. The fluorescence lifetimes for **PS1** and **PS2** were found to be 1.90 ns and 3.51 ns, respectively (Fig. S29 and S30, ESI†). Subsequently, the reductive quenching rate constants (k_q) for **PS1** and **PS2** in the presence of BIH in DMF were determined to be 8.37×10^9 M^{-1} s^{-1} and 1.19×10^9 M^{-1} s^{-1}, respectively, based on the Stern–Volmer equation (Fig. S31 and S32, ESI†). In contrast, the oxidative quenching k_q could not be obtained due to significant spectral overlap of the Fe catalyst at both excitation and emission wavelengths (Fig. S33, ESI†), which has been observed in the literature.[9] However, the substantial excess of BIH (over five orders of magnitude than the catalyst) and the fast reductive quenching k_q both suggest the photocatalytic pathway follows a reductive quenching mechanism (Scheme 1). By monitoring the UV-vis spectra of

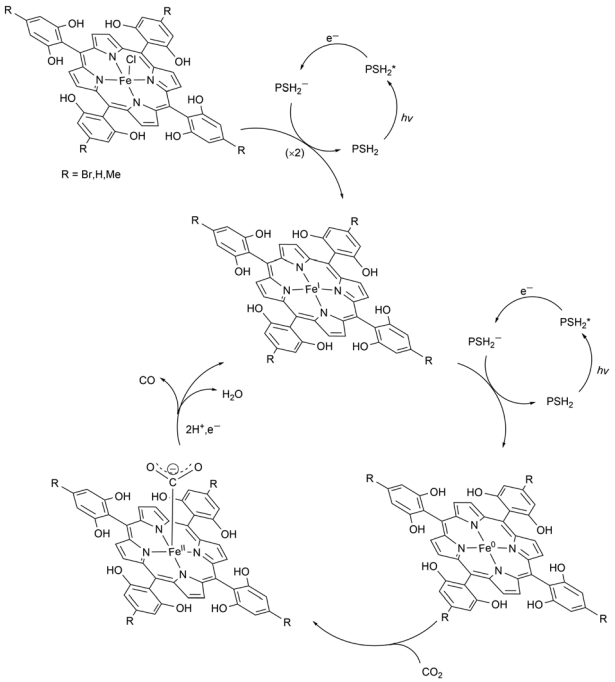

Scheme 1 Proposed mechanism for photocatalytic CO_2 reduction with iron porphyrins.

PS1 and **PS2** during photocatalytic reduction of CO_2 (Fig. S34 and S35, ESI†), we observed intermediates at ~400 nm, which were consistent with a $3e^-/2H^+$ photoproduct PSH_2^- (Scheme 1) previously proposed by our laboratory.[7b,10] This intermediate has been found to be highly reducing and critical in electron transfer to the Fe catalyst for CO_2 reduction.[7b]

The UV-vis spectra of **Fe1** and **Fe3** showed fast conversion of the Fe(III) compound (416 nm) to an Fe(II) species (432 nm) within one minute, which subsequently transformed into an Fe(I) species (420 nm) (Fig. 4 and Scheme 1). This Fe(I) species decreased slowly during the CO_2 reduction process. These observations are consistent with the photocatalytic mechanism previously delineated by Robert *et al.* when using **Fe2** as the CO_2 reduction catalyst.[7b,11] However, the identical reduction processes observed for both **Fe1** and **Fe3** suggest that these steps (from Fe^{3+} to Fe^+) are not rate-determining in photocatalysis. As detailed by Robert *et al.*, the production of CO is closely related to the formation and stability of an Fe(II)CO_2 adduct

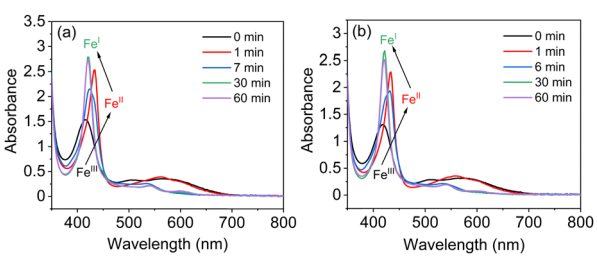

Fig. 4 UV-vis spectra of systems containing 30 mM BIH, 20 μM **PS1**, 20 μM **Fe1** (a) or 20 μM **Fe3** (b) in DMF under CO_2, upon irradiation with blue LED light.

(generated from Fe^0 and CO_2).[9a,12] The –OH groups on the porphyrin ring enhance the stability of Fe(II)CO_2 adduct *via* internal hydrogen bonding interaction. Further reduction instead of protonation of the Fe(II)CO_2 for cleaving the C–O bond was found to be more favorable in **Fe2** than the non-substituted tetraphenylporphyrin Fe complex.[11a] Thus, the reduction steps either from Fe(I) to Fe(0) or from Fe(II)CO_2 to Fe(I) could be rate-determining in photocatalytic CO_2 reduction (Scheme 1).

The present study showed that the catalytic activity significantly depends on the ligand electronic factors: a faster rate in CO generation was observed with an Fe catalyst having more electron-withdrawing groups (Table 1). A rationalization of the observation is that the more electron-withdrawing ligand facilitates the reduction of Fe(I) or Fe(II)CO_2. Both steps are essential in generation of the requisite Fe(0) intermediate and in the cleavage of C–O bond for CO_2 reduction. Indeed, the onset catalytic potentials of Fe complexes shift slightly towards more positive values for the ones with more electron-withdrawing substituents (Table 1).

In this study, we designed and synthesized two novel iron porphyrin complexes, **Fe1** and **Fe3**, which incorporate electron-withdrawing -Br and electron-donating -Me groups. By employing cost-effective anthraquinone photosensitizers (**PS1** and **PS2**) in noble-metal-free systems, we evaluated the activity of these Fe catalysts in photocatalytic CO_2 reduction, achieving a high TON of 10 476 in CO production with selectivity reaching 100%. Importantly, the results reveal that the activity for CO production follows the trend of **Fe1** > **Fe2** > **Fe3**, aligning with the onset catalytic potential of $Fe^{I/0}$. This suggests that the reduction of Fe catalyst especially from Fe(I) to Fe(0) is probably the rate-determining step in photocatalysis. This work thus offers new insights for the development of precious metal-free photocatalytic systems for CO_2 reduction.

We are grateful for the financial support provided by Sun Yat-sen University, GBRCE for Functional Molecular Engineering, Jiaying University, and the China Postdoctoral Science Foundation (2022TQ0380 H. Y.; 2022M723586 H. Y.).

Conflicts of interest

There are no conflicts to declare.

Notes and references

1 (*a*) X. Liu, S. Inagaki and J. Gong, *Angew. Chem., Int. Ed.*, 2016, **55**, 14924–14950; (*b*) R. Francke, B. Schille and M. Roemelt, *Chem. Rev.*, 2018, **118**, 4631–4701; (*c*) J. Lv, J. Xie, A. G. A. Mohamed, X. Zhang, Y. Feng, L. Jiao, E. Zhou, D. Yuan and Y. Wang, *Nat. Rev. Chem.*, 2023, **7**, 91–105.

2 (*a*) J. Y. Y. Loh, N. P. Kherani and G. A. Ozin, *Nat. Sustainability*, 2021, **4**, 466–473; (*b*) B. Su, Y. Kong, S. Wang, S. Zuo, W. Lin, Y. Fang, Y. Hou, G. Zhang, H. Zhang and X. Wang, *J. Am. Chem. Soc.*, 2023, **145**, 27415–27423.

3 (*a*) K. E. Dalle, J. Warnan, J. J. Leung, B. Reuillard, I. S. Karmel and E. Reisner, *Chem. Rev.*, 2019, **119**, 2752–2875; (*b*) R. N. Sampaio, D. C. Grills, D. E. Polyansky, D. J. Szalda and E. Fujita, *J. Am. Chem. Soc.*, 2020, **142**, 2413–2428; (*c*) H. Shirley, X. Su, H. Sanjanwala, K. Talukdar, J. W. Jurss and J. H. Delcamp, *J. Am. Chem. Soc.*, 2019, **141**, 6617–6622; (*d*) P. L. Cheung, S. C. Kapper, T. Zeng, M. E. Thompson and C. P. Kubiak, *J. Am. Chem. Soc.*, 2019, **141**, 14961–14965; (*e*) T. Ouyang, H.-J. Wang, H.-H. Huang, J.-W. Wang, S. Guo, W.-J. Liu, D.-C. Zhong and T.-B. Lu, *Angew. Chem., Int. Ed.*, 2018, **57**, 16480–16485; (*f*) K. Kamada, J. Jung, T. Wakabayashi, K. Sekizawa, S. Sato, T. Morikawa, S. Fukuzumi and S. Saito, *J. Am. Chem. Soc.*, 2020, **142**, 10261–10266; (*g*) Y. Hameed, P. Berro, B. Gabidullin and D. Richeson, *Chem. Commun.*, 2019, **55**, 11041–11044; (*h*) N. P. Liyanage, W. Yang, S. Guertin, S. Sinha Roy, C. A. Carpenter, R. E. Adams, R. H. Schmehl, J. H. Delcamp and J. W. Jurss, *Chem. Commun.*, 2019, **55**, 993–996; (*i*) A. Genoni, D. N. Chirdon, M. Boniolo, A. Sartorel, S. Bernhard and M. Bonchio, *ACS Catal.*, 2017, **7**, 154–160; (*j*) D. Hong, Y. Tsukakoshi, H. Kotani, T. Ishizuka and T. Kojima, *J. Am. Chem. Soc.*, 2017, **139**, 6538–6541; (*k*) H. Rao, L. C. Schmidt, J. Bonin and M. Robert, *Nature*, 2017, **548**, 74–77; (*l*) D.-C. Liu, Z.-M. Luo, B. M. Aramburu-Trošelj, F. Ma and J.-W. Wang, *Chem. Commun.*, 2023, **59**, 14626–14635.

4 (*a*) C.-F. Leung and T.-C. Lau, *Energy Fuels*, 2021, **35**, 18888–18899; (*b*) B. Su, M. Zheng, W. Lin, X. F. Lu, D. Luan, S. Wang and X. W. Lou, *Adv. Energy Mater.*, 2023, **13**, 2203290; (*c*) G. Chen, Z. Zhou, B. Li, X. Lin, C. Yang, Y. Fang, W. Lin, Y. Hou, G. Zhang and S. Wang, *J. Environ. Sci.*, 2024, **140**, 103–112.

5 (*a*) P.-Y. Ho, S.-C. Cheng, F. Yu, Y.-Y. Yeung, W.-X. Ni, C.-C. Ko, C.-F. Leung, T.-C. Lau and M. Robert, *ACS Catal.*, 2023, **13**, 5979–5985; (*b*) S. E. Lee, A. Nasirian, Y. E. Kim, P. T. Fard, Y. Kim, B. Jeong, S.-J. Kim, J.-O. Baeg and J. Kim, *J. Am. Chem. Soc.*, 2020, **142**, 19142–19149; (*c*) Y. Wang, T. Liu, L. Chen and D. Chao, *Inorg. Chem.*, 2021, **60**, 5590–5597; (*d*) H. Takeda, K. Ohashi, A. Sekine and O. Ishitani, *J. Am. Chem. Soc.*, 2016, **138**, 4354–4357; (*e*) A. Rosas-Hernández, C. Steinlechner, H. Junge and M. Beller, *Green Chem.*, 2017, **19**, 2356–2360; (*f*) Y. Sakaguchi, A. Call, M. Cibian, K. Yamauchi and K. Sakai, *Chem. Commun.*, 2019, **55**, 8552–8555; (*g*) X. Zhang, K. Yamauchi and K. Sakai, *ACS Catal.*, 2021, **11**, 10436–10449; (*h*) J.-W. Wang, X. Zhang, L. Velasco, M. Karnahl, Z. Li, Z.-M. Luo, Y. Huang, J. Yu, W. Hu, X. Zhang, K. Yamauchi, K. Sakai, D. Moonshiram and G. Ouyang, *JACS Au*, 2023, **3**, 1984–1997; (*i*) L.-L. Gracia, L. Luci, C. Bruschi, L. Sambri, P. Weis, O. Fuhr and C. Bizzarri, *Chem. – Eur. J.*, 2020, **26**, 9929–9937; (*j*) H. Takeda, H. Kamiyama, K. Okamoto, M. Irimajiri, T. Mizutani, K. Koike, A. Sekine and O. Ishitani, *J. Am. Chem. Soc.*, 2018, **140**, 17241–17254.

6 (*a*) E. E. Benson, C. P. Kubiak, A. J. Sathrum and J. M. Smieja, *Chem. Soc. Rev.*, 2009, **38**, 89–99; (*b*) C. Costentin, S. Drouet, M. Robert and J.-M. Savéant, *Science*, 2012, **338**, 90–94.

7 (*a*) H. Yuan, B. Cheng, J. Lei, L. Jiang and Z. Han, *Nat. Commun.*, 2021, **12**, 1835; (*b*) Q. Lei, H. Yuan, J. Du, M. Ming, S. Yang, Y. Chen, J. Lei and Z. Han, *Nat. Commun.*, 2023, **14**, 1087.

8 A. Stoumpidi, A. Trapali, M. Poisson, A. Barrozo, S. Bertaina, M. Orio, G. Charalambidis and A. G. Coutsolelos, *ChemCatChem*, 2023, **15**, e202200856.

9 (*a*) J. Bonin, M. Robert and M. Routier, *J. Am. Chem. Soc.*, 2014, **136**, 16768–16771; (*b*) H. Rao, J. Bonin and M. Robert, *ChemSusChem*, 2017, **10**, 4447–4450.

10 M. Kuss-Petermann, M. Orazietti, M. Neuburger, P. Hamm and O. S. Wenger, *J. Am. Chem. Soc.*, 2017, **139**, 5225–5232.

11 (*a*) J. Bonin, A. Maurin and M. Robert, *Coord. Chem. Rev.*, 2017, **334**, 184–198; (*b*) H. Rao, J. Bonin and M. Robert, *Chem. Commun.*, 2017, **53**, 2830–2833.

12 J. Bonin, M. Chaussemier, M. Robert and M. Routier, *ChemCatChem*, 2014, **6**, 3200–3207.